Dalton Transactions

ROYAL SOCIETY OF CHEMISTRY

PAPER

View Article Online
View Journal | View Issue

Cite this: *Dalton Trans.*, 2023, **52**, 10109

Synthesis and characterization of a new rare earth borate nonlinear optical crystal $K_7PbLu_2B_{15}O_{30}$†

Juhe Liu,[a,c,d] Yuwei Chen,[a,b,d] Mengran Sun,[a,b,d] Wenhao Liu,[a,b,d] Xianghe Meng*[a,d] and Jiyong Yao*[a,b]

Received 6th June 2023,
Accepted 27th June 2023

DOI: 10.1039/d3dt01740k

rsc.li/dalton

A new complex rare earth borate $K_7PbLu_2B_{15}O_{30}$ was prepared by the spontaneous crystallization method. $K_7PbLu_2B_{15}O_{30}$ is crystallized in the chiral trigonal space group *R*32 with cell parameters $a = b = 13.0893(3)$ Å, $c = 15.2379(6)$ Å, $\alpha = \beta = 90°$, $\gamma = 120°$, and $Z = 3$. The basic structure of the crystal can be seen as composed of B_5O_{10} groups and LuO_6 polyhedra sharing oxygen atoms, while K^+ and Pb^{2+} fill the space to balance the charge. The UV transmission cut-off edge of $K_7PbLu_2B_{15}O_{30}$ was less than 300 nm, and the powder SHG response was roughly 1.1 times that of KDP. Furthermore, a first-principles analysis was performed to see more about the relationship between the crystal structure and optical characteristics.

Introduction

Nonlinear optical (NLO) materials have an important role in lithography, semiconductor manufacturing, and laser technology.[1–8] Over the past few decades, with continuous efforts, scientists have developed many commercially available NLO materials for application in the ultraviolet to mid-infrared regions, for example BaB_2O_4(BBO),[9] LiB_3O_5(LBO),[10] KH_2PO_4(KDP),[11] $KTiOPO_4$(KTP),[12] $AgGaQ_2$ (Q = S, Se),[13,14] $ZnGeP_2$ (ZGP),[15] $LiGaS_2$,[16] $LiInSe_2$,[17] and GaSe.[18] In general, the following specifications must also be satisfied for a NLO crystal with suitable performance:[19] a non-centrosymmetric space group to perform the NLO function, an enough effective NLO coefficient ($d_{eff} > 0.39$ pm V^{-1}), a wide band gap ($E_g > 6.2$ eV) and an acceptable birefringence (0.05–0.1) to achieve phase matching. Borate compounds have long been recognized as the material of choice for the ultraviolet (UV) and deep ultraviolet (DUV) regions due to their unique structural characteristics and performance advantages. Firstly, in borates, the B and O atoms can be tri- or tetra-ligated to form two fundamental structural units, BO_3 and BO_4.[20–22] Through sharing O atoms, these two types of units can form other characteristic groups. The most prevalent ones are B_2O_5, B_3O_6, B_3O_7, B_4O_9, B_5O_{10}, and B_8O_{15} units.[23–30] The rich structure type of borates is very favorable to produce compounds with non-centrosymmetric structures. Moreover, borates can be used in the UV/DUV area due in large part to the significant electronegativity difference between the B and O elements, which is very beneficial for improving the transmission of crystals at short wavelengths and increasing the laser damage threshold. In particular, the BO_3 group is particularly conducive to producing substantial microscopic secondary polarizability because of the existence of conjugated π-orbitals and a highly anisotropic electron distribution.[31,32]

In general, alkali/alkaline earth metal elements and partial rare earth metal elements (Sc^{3+}, Y^{3+}, La^{3+}, Lu^{3+}) without d–d and f–f electronic transitions are usually introduced into the borate system to provide materials with shorter cut-off edges.[33–35] In addition, effective strategies have been adopted to enhance the SHG and birefringence of materials, such as introducing the local polarities of asymmetric building units, including distorted polyhedra with active lone pairs, such as Pb^{2+}, Sn^{2+}, Sb^{3+}, Bi^{3+}, *etc.*[36–39] The combination of alkali/alkaline earth/partial rare earth elements, distorted polyhedra with active lone pairs and B–O anionic groups can coordinate the comprehensive performance of NLO crystals and balance the relationship between the bandgap, birefringence, and NLO effect.

In line with the aforementioned concept, a new non-centrosymmetric borate $K_7PbLu_2B_{15}O_{30}$ was synthesized through the spontaneous crystallization method. In this paper, the syntheses, structures, thermal behavior, UV-Vis-NIR spectrum and

[a]*Beijing Center for Crystal Research and Development, Key Lab of Functional Crystals and Laser Technology, Technical Institute of Physics and Chemistry, Chinese Academy of Sciences, Beijing 100190, P. R. China. E-mail: jyao@mail.ipc.ac.cn, mengxianghe@mail.ipc.ac.cn*

[b]*Center of Materials Science and Optoelectronics Engineering, University of Chinese Academy of Sciences, Beijing 100049, P. R. China*

[c]*School of Future Technology, University of Chinese Academy of Sciences, Beijing, 100049, China*

[d]*University of Chinese Academy of Sciences, Beijing 100049, P. R. China*

†Electronic supplementary information (ESI) available: Experimental and simulated PXRD patterns, TG-DSC curves, a comparison diagram of XRD before and after melting of the compound $K_7PbLu_2B_{15}O_{30}$, and crystallographic data. CCDC 2261770. For ESI and crystallographic data in CIF or other electronic format see DOI: https://doi.org/10.1039/d3dt01740k

NLO characteristics of the title compound are described. In order to better understand the relationship between the crystal structure and performance, first-principles analysis was also performed.

Experimental section

Single crystal growth

Single crystals of $K_7PbLu_2B_{15}O_{30}$ were obtained through the spontaneous crystallization method. KF (99.9%, Aladdin), PbF_2 (99.5%, Aladdin), Lu_2O_3 (99.9%, Aladdin), and B_2O_3 (99.99%, Aladdin) were mixed in a platinum crucible in a 6 : 1 : 1 : 15 molar ratio. After grinding, the mixed raw materials were put into the furnace and the temperature was raised from room temperature to 950 °C at a rate of 1 °C min^{-1} and kept for 1 day. Subsequently, after 6 days, the temperature was cooled to 750 °C. Finally, it was naturally cooled to room temperature.

Synthesis of polycrystalline powder

Polycrystalline samples of $K_7PbLu_2B_{15}O_{30}$ were prepared by the high-temperature solid-phase method. The reaction raw materials (K_2CO_3, PbO, Lu_2O_3, H_3BO_3) were weighed according to the stoichiometric molar ratio, carefully ground in an agate mortar and put into a platinum crucible. The reaction was then carried out as follows: calcination at 300 °C for 1 day, grinding again, and then heating to 830 °C for 3 days to obtain the target compound. The sample was pure, as it was verified by powder X-ray diffraction (PXRD) analysis (Fig. S1†).

Powder X-ray diffraction (PXRD)

The PXRD data of the powder sample were obtained at room temperature using a Bruker D8 focus diffractometer with Cu Kα radiation (λ = 1.5418). The test parameters are 0.02° for the scan step width, 0.1 s per step for the scan speed, and 10–50° for the 2θ range.

Single-crystal structure determination

A single crystal X-ray diffractometer was used to determine the crystal structure. With a Rigaku AFC10 diffraction device, diffraction data for the target compound were obtained using graphite monochromatic Mo-Kα (λ = 0.71073 Å) radiation at room temperature. The CrysAlispro program[40] and the Multiscan method were used for data collection and absorption correction. The crystal structure for the target compound was resolved directly with the ShelXT[41] program, and the structure of the crystal was optimized with ShelXL[42] using full matrix least squares minimization on F^2. Table 1 lists the crucial structural parameters for $K_7PbLu_2B_{15}O_{30}$.

Spectroscopy

The Varian Excalibur 3000 Fourier transform infrared (IR) spectrometer was used to study the infrared spectra of $K_7PbLu_2B_{15}O_{30}$ in the 400–3000 cm^{-1} range. The target compound powder sample was mixed with KBr at a mass ratio of 1 : 100 in order to prepare for an IR spectrometer test. To identify the absorption edge of $K_7PbLu_2B_{15}O_{30}$, the UV-vis-NIR diffuse reflectance spectrum for $K_7PbLu_2B_{15}O_{30}$ powder samples was obtained using a Shimadzu UV-3600i Plus spectrophotometer.

Table 1 Crystal data and structure refinement for $K_7PbLu_2B_{15}O_{30}$

Empirical formula	$K_7PbLu_2B_{15}O_{30}$
Formula weight	1472.98
Temperature/K	273.15
Crystal system	Trigonal
Space group	*R*32
a/Å	13.0893(3)
b/Å	13.0893(3)
c/Å	15.2379(6)
α/°	90
β/°	90
γ/°	120
Volume/$Å^3$	2260.94(14)
Z	3
ρ_{calc}/g cm^{-3}	3.245
μ/mm^{-1}	13.153
F (000)	2016.0
Crystal size	0.4 × 0.7 × 0.9 mm^3
Radiation	Mo Kα (λ = 0.71073)
2Θ range for data collection (°)	4.478 to 55.1
Index ranges	$-16 \le h \le 16$, $-16 \le k \le 16$, $-19 \le l \le 19$
Reflections collected	13 236
Independent reflections	1167 [R_{int} = 0.0885, R_{sigma} = 0.0404]
Data/restraints/parameters	1167/0/88
Goodness-of-fit on F^2	1.170
Final *R* indexes [$I \ge 2\sigma(I)$][a]	R_1 = 0.0218, wR_2 = 0.0511
Final *R* indexes [all data][a]	R_1 = 0.0258, wR_2 = 0.0516
Largest diff. peak/hole/e $Å^{-3}$	1.04/−1.69

[a] $R_1 = \sum||F_o| - |F_c||/\sum|F_o|$, and w$R_2 = [\sum w(F_o^2 - F_c^2)2/\sum wF_o^4]^{1/2}$ for $F_o^2 > 2\sigma(F_o^2)$.

SHG tests

The Kurtz and Perry[43] technique was used to investigate the powder SHG effect of $K_7PbLu_2B_{15}O_{30}$. The fundamental frequency light at 1064 nm for the test was produced using a Q-switched Nd:YAG laser. $K_7PbLu_2B_{15}O_{30}$ polycrystalline powder was finely ground. Then, the following particle size ranges are selected: 50–100, 100–150, 150–200, 200–250, and 250–300 μm. For comparison, crystalline KDP samples were milled in the same manner.

Thermal analysis

The thermal properties of $K_7PbLu_2B_{15}O_{30}$ were determined by differential scanning calorimetric (DSC) analysis and thermogravimetric analysis (TGA) with the use of a thermal analyzer NETZSCH STA 409C/CD. The samples were initially heated at a rate of 10° min^{-1} to 1100 °C under a N_2 atmosphere, and then they were cooled at the same rate to room temperature.

Computational method

Based on the DFT theory, the electronic structure of $K_7PbLu_2B_{15}O_{30}$ was calculated in the CASTEP software package using the method of the plane wave pseudopotential.[44–47] The

PBE (Perdew, Burke, and Ernzerhof) functionals of the generalized gradient approximation (GGA) were used to represent the exchange–correlation effect.[48] Under the norm-conserving pseudopotential (NCP),[49] the following orbital electrons were treated as valence electrons: K, $3s^2 3p^6 4s^1$, Pb, $5d^{10} 6s^2 6p^2$, Lu, $4f^{14} 5d^1 6s^2$, B, $2s^2 2p^1$, O, $2s^2 2p^4$. The plane wave energy cutoff is set at 750 eV to achieve energy convergence. The step of k points in the Monkhorst–Pack within the Brillouin zone was selected as 0.04 $Å^{-3}$ to ensure the accuracy of the results. Also, based on the experimentally acquired crystal structure data, the theoretical band gaps, DOS and PDOS density maps, and birefringence values of the materials were simulated.

Results and discussion

Structure description

$K_7PbLu_2B_{15}O_{30}$ crystallizes in the chiral trigonal space group $R32$ with the unit cell parameters $a = b = 13.0893(3)$ Å, $c = 15.2379(6)$ Å, $\alpha = \beta = 90°$, $\gamma = 120°$ and $Z = 3$. The substance features a three-dimensional network structure made of KO_6, KO_8, PbO_6 (Fig. S2†), LuO_6 polyhedra, and B_5O_{10} units. Each isolated B_5O_{10} unit consists of a BO_4 tetrahedral unit and four BO_3 triangular units (Fig. 1a). Four terminal O atoms connect each isolated B_5O_{10} group to separate LuO_6 octahedra, forming a complex three-dimensional network (Fig. 1b). K ions and Pb ions are filled in the voids to balance the charge (Fig. 1c). In the B_5O_{10} group, the bond length between the B atom and the O atom ranges from 1.329 Å to 1.473 Å. The B–O bond length in the BO_4 group is longer than the B–O bond length in the BO_3 group, which is consistent with the typical B–O bond distance, as shown in Table S1.† The distance between the Pb atom and the six surrounding O atoms is 2.503(7) Å, and the Lu atom is in the range of 2.182 Å to 2.296 Å away from the surrounding O atoms. In addition, the total bond valences (BVS) of $K_7PbLu_2B_{15}O_{30}$ crystals were calculated for the K, Pb, Lu, and B elements as follows 1.23(K1), 0.95(K2), 0.94(K3), 2.10(Pb), 2.92(Lu), 3.08(B1), 2.99(B2), 2.94(B3). This shows the +1, +2, +3, and +3 valence states for K, Pb, Lu, and B, respectively, in the $K_7PbLu_2B_{15}O_{30}$ crystal.

Thermal stability

TG and DSC were used to assess the thermal stabilities of the polycrystalline $K_7PbLu_2B_{15}O_{30}$ samples. Only one endothermic peak appears on the heating DSC curves, and there is no obvious weight loss seen on the TG curves in the temperature range of 30–1000 °C, suggesting that the tested compound is stable at least up to 898 °C (Fig. S3†). Due to the high viscosity of the B-rich system, there are no peaks on the cooling portion of the DSC curves. Moreover, the incongruent melting behavior of the compound was determined by comparing the re-crystallized product after melting with the original samples (Fig. S4†).

Optical properties

The infrared spectrum was studied to define the coordination model of the B atoms in $K_7PbLu_2B_{15}O_{30}$. The absorption peak at 2360 cm^{-1} in Fig. S5† is supposed to be an impurity peak associated with airborne carbon dioxide. Contrary to relevant literature,[21] it is found that the absorption peak at the position of 1359 cm^{-1}, 1252 cm^{-1}, and 1196 cm^{-1} belongs to the asymmetric stretching vibration peak of the BO_3 unit. The absorption peak at 1030 cm^{-1} position belongs to the asymmetric stretching vibration of the BO_4 unit. The absorption peak at

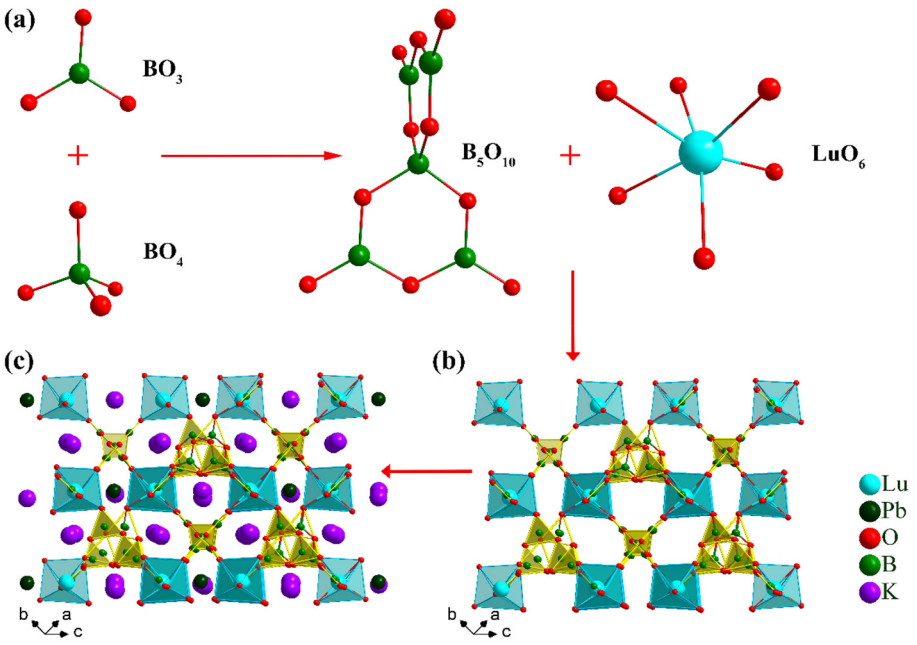

Fig. 1 (a) BO_3, BO_4, B_5O_{10}, and LuO_6 groups. (b) 3D structure formed by LuO_6 and B_5O_{10} groups. (c) Whole 3D crystal structure of $K_7PbLu_2B_{15}O_{30}$.

938 cm^{-1} position belongs to the symmetrical stretching vibration of the BO_3 unit. The absorption peak at 780 cm^{-1} position belongs to the symmetrical stretching vibration of the BO_4 unit. These distinctive peaks in the infrared spectrum show that BO_3 and BO_4 groups are present in the structure of $K_7PbLu_2B_{15}O_{30}$. The UV-vis-NIR diffuse reflectance spectrum and the second harmonic generation (SHG) effects are displayed in Fig. 2. The cutoff edge is about 300 nm, which is consistent with some previously reported UV cutoff edges of Pb compounds, such as $Li_2PbB_2O_5$,[50] Pb_2BO_3Cl,[51] Pb_2BO_3I,[52] and $Pb_2Ba_3(BO_3)_3Cl$.[33] The SHG effect of powder compounds at discrete particle sizes is characterized using the Kurtz and Perry technique to evaluate its NLO properties with KDP as a reference. The experimental results show that the SHG intensity of $K_7PbLu_2B_{15}O_{30}$ is about 1.1 times that of KDP. The nonlinear strength of $K_7PbLu_2B_{15}O_{30}$ steadily increases with the particle size and eventually approaches saturation, demonstrating the crystal's type-1 phase matching capability.

Electronic structure calculations

First-principles calculations were performed on the compound to shed light on the relationship between the atomic structure of matter and its macroscopic qualities. As inferred from the calculated energy band structure, $K_7PbLu_2B_{15}O_{30}$ is an indirect band gap material with a band gap value of 4.052 eV. The valence band maximum (VBM) and conduction band minimum (CBM) of $K_7PbLu_2B_{15}O_{30}$ are at Γ point and G point, respectively (Fig. 3a). Due to a break in the exchange correlation energy functional used in the theoretical calculation, the calculated band gap value is smaller than the experimental band gap value. From the total and partial density of states (Fig. 3b) of $K_7PbLu_2B_{15}O_{30}$, we can draw the following conclusions: the VB from −20 to −15 eV is mainly composed of the B 2s 2p, and O 2s orbitals, primarily as a result of the B and O hybridization in the B_5O_{10} unit. The VB from −15 to −5 eV is mainly composed of the K 3p, Pb 5d, B 2s 2p, and O 2p

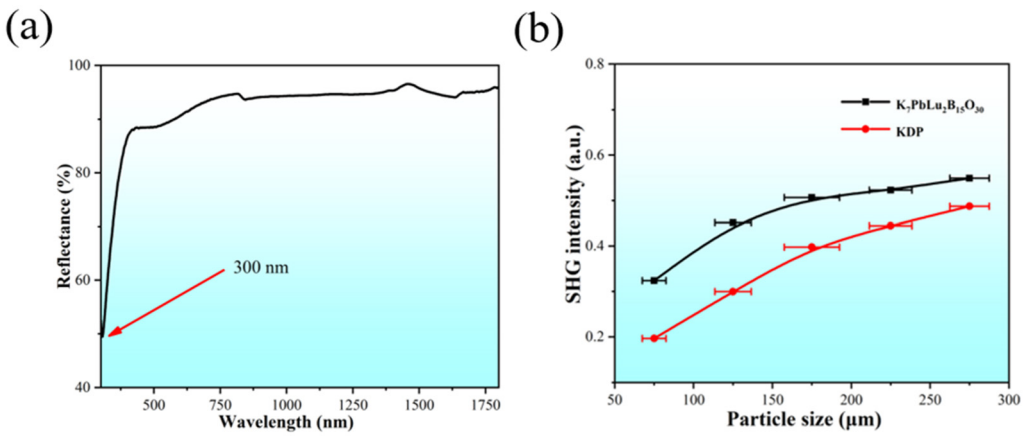

Fig. 2 (a) UV–vis–NIR diffuse reflectance spectrum of powder $K_7PbLu_2B_{15}O_{30}$. (b) SHG intensity curve with different particle sizes.

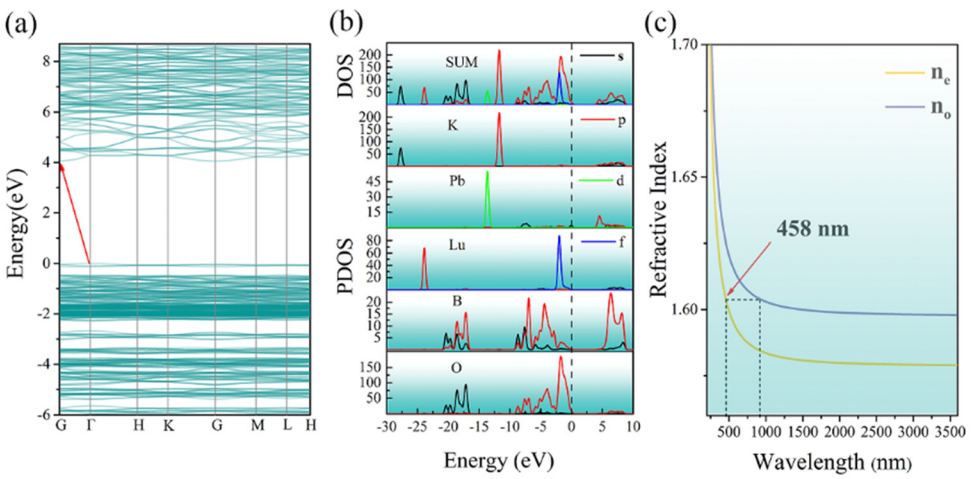

Fig. 3 (a) Calculated electronic energy band structure. (b) DOS and PDOS. (c) Calculated dispersive refractive indices in $K_7PbLu_2B_{15}O_{30}$.

orbitals, which helps in the formation of the K–O, Pb–O, and B–O bonds in the structure. From −5 eV to VBM, these bands come mainly from the B 2p, Lu 4f, and O 2p orbitals. The CB bottom is mainly consisting of the Pb 6p, B 2s and B 2p orbitals. The results of the above analysis show that the synergies between the Pb–O group and Lu–O polyhedra and the B_5O_{10} unit affect the optical properties of the material. The birefringence (Δn) calculated for the title compound is ~0.0224@1064 nm (Fig. 3c). The value is not in the typical suitable range (0.05–0.1) for implementing phase matching. $K_7PbLu_2B_{15}O_{30}$ is a trigonal uniaxial crystal, and it is possible to obtain the shortest $n_e(\omega) = n_o(2\omega)$ at 458 nm, demonstrating that the shortest phase matching wavelength of $K_7PbLu_2B_{15}O_{30}$ is 458 nm. Even though $K_7PbLu_2B_{15}O_{30}$ has a small birefringence, it still has the ability to maintain phase matching at 1064 nm, which is in line with the testing results.

Conclusions

A new rare-earth borate $K_7PbLu_2B_{15}O_{30}$ was synthesized through spontaneous crystallization. The title compound has a wide transparency range and a short cut edge in the UV range. The compound has a large SHG intensity comparable to that of KDP and can show phase matching by using a 1064 nm laser light source. First-principles simulations showed that the optical properties result from the interactions of the PbO_6, LuO_6, and B_5O_{10} units. This research adds to the richness of the rare-earth borate system and offers a potential NLO crystal in the ultraviolet region.

Author contributions

Juhe Liu: experimental testing and writing of the original draft. Yuwei Chen: data analysis. Mengran Sun: theoretical analysis. Wenhao Liu: data analysis. Xianghe Meng: writing and revising. Jiyong Yao: writing, experimental design, and overall contactor.

Conflicts of interest

The authors declare no competing financial interest.

Acknowledgements

This work was supported by the National Natural Science Foundation of China (no. 22175190, 51890862) and the CAS Specific Research Assistant Funding Program (292060000).

References

1 S. Liang and W. Sun, *Adv. Mater. Technol.*, 2022, **7**, 2101502.
2 A. Takada, K. Matsushita, S. Horioka, Y. Furuichi and Y. Sumi, *BMC Oral Health*, 2017, **17**, 96.
3 L. E. Sánchez-Cadena, G. Tersac, X. Coqueret and Z. Gamiño-Arroyo, *Prog. Org. Coat.*, 2019, **136**, 105268.
4 S. Peng, L. Liu, L. Wang, R. Rong, L. Song, W. You, J. Shi and Y. Zhang, *J. Rare Earths*, 2022, **40**, 1417–1423.
5 N. Augsburger, A. T. Rachmadi, N. Zaouri, Y. Lee and P.-Y. Hong, *Environ. Sci. Technol.*, 2021, **55**, 16283–16298.
6 Z. H. Kang, J. Guo, Z. S. Feng, J. Y. Gao, J. J. Xie, L. M. Zhang, V. Atuchin, Y. Andreev, G. Lanskii and A. Shaiduko, *Appl. Phys. B: Lasers Opt.*, 2012, **108**, 545–552.
7 S. A. Bereznaya, Z. V. Korotchenko, R. A. Redkin, S. Y. Sarkisov, V. N. Brudnyi, A. V. Kosobutsky and V. V. Atuchin, *Infrared Phys. Technol.*, 2016, **77**, 100–103.
8 I. S. Steinberg, A. V. Kirpichnikov and V. V. Atuchin, *Opt. Mater.*, 2018, **78**, 253–258.
9 C. T. Chen, B. C. Wu, A. D. Jiang and G. M. You, *Sci. Sin., Ser. B*, 1985, **28**, 235–243.
10 C. T. Chen, Y. C. Wu, A. D. Jiang, B. C. Wu, G. M. You, R. K. Li and S. J. Lin, *J. Opt. Soc. Am. B*, 1989, **6**, 616–621.
11 B. Březina and M. Havránková, *Mater. Res. Bull.*, 1971, **6**, 537–543.
12 S. Dezhong and H. Chaoen, *Prog. Cryst. Growth Charact.*, 1985, **11**, 269–274.
13 A. H. Akiko Harasaki and K. K. Kiyoshi Kato, *Jpn. J. Appl. Phys.*, 1997, **36**, 700.
14 B. Tell and H. M. Kasper, *Phys. Rev. B: Solid State*, 1971, **4**, 4455–4459.
15 G. D. Boyd, E. Buehler and F. G. Storz, *Appl. Phys. Lett.*, 1971, **18**, 301–304.
16 V. V. Atuchin, L. I. Isaenko, V. G. Kesler and S. I. Lobanov, *J. Alloys Compd.*, 2010, **497**, 244–248.
17 V. V. Atuchin, L. I. Isaenko, S. I. Lobanov, A. A. Goloshumova, M. S. Molokeev, Z. Zhang, X. Zhang, X. Jiang and Z. Lin, *Molecules*, 2022, **27**, 5078.
18 Z.-S. Feng, Z.-H. Kang, F.-G. Wu, J.-Y. Gao, Y. Jiang, H.-Z. Zhang, Y. M. Andreev, G. V. Lanskii, V. V. Atuchin and T. A. Gavrilova, *Opt. Express*, 2008, **16**, 9978–9985.
19 M. Mutailipu, M. Zhang, Z. Yang and S. Pan, *Acc. Chem. Res.*, 2019, **52**, 791–801.
20 C. Chen, Y. Wu and R. Li, *Int. Rev. Phys. Chem.*, 2008, **8**, 65–91.
21 M. Mutailipu, Z. Xie, X. Su, M. Zhang, Y. Wang, Z. Yang, M. R. S. A. Janjua and S. Pan, *J. Am. Chem. Soc.*, 2017, **139**, 18397–18405.
22 Y. Chen, J. Feng, F. Fan, J. Shen, G. Zhang and H. Tu, *J. Solid State Chem.*, 2023, **320**, 123835.
23 X. Meng, M. Xia and R. Li, *New J. Chem.*, 2019, **43**, 11469–11472.
24 W.-J. Xie, Z. Fang and J.-G. Mao, *Inorg. Chem.*, 2022, **61**, 18260–18266.
25 S. Guo, W. Zhang, M. Zhang, Z. Yang and S. Pan, *Inorg. Chem.*, 2021, **60**, 883–891.
26 Y. Chen, W. Liu, J. Feng, R. Guo, F. Fan, J. Shen, G. Zhang and H. Tu, *Cryogenics*, 2022, 103476.
27 J. Liu, M.-H. Lee, C. Li, X. Meng and J. Yao, *Inorg. Chem.*, 2022, **61**, 19302–19308.

28 V. V. Atuchin, B. G. Bazarov, T. A. Gavrilova, V. G. Grossman, M. S. Molokeev and Z. G. Bazarova, *J. Alloys. Compd.*, 2012, **515**, 119–122.
29 V. V. Atuchin, V. G. Kesler, A. I. Zaitsev, M. S. Molokeev, A. S. Aleksandrovsky, A. A. Kuzubov and N. Y. Ignatova, *J. Phys.: Condens. Matter*, 2013, **25**, 085503.
30 V. V. Atuchin, A. K. Subanakov, A. S. Aleksandrovsky, B. G. Bazarov, J. G. Bazarova, T. A. Gavrilova, A. S. Krylov, M. S. Molokeev, A. S. Oreshonkov and S. Y. Stefanovich, *Mater. Des.*, 2018, **140**, 488–494.
31 J.-L. Song, C.-L. Hu, X. Xu, F. Kong and J.-G. Mao, *Angew. Chem., Int. Ed.*, 2015, **54**, 3679–3682.
32 Y. Song, M. Luo, F. Liang, N. Ye and Z. Lin, *Chem. Commun.*, 2018, **54**, 1445–1448.
33 X. Dong, Q. Jing, Y. Shi, Z. Yang, S. Pan, K. R. Poeppelmeier, J. Young and J. M. Rondinelli, *J. Am. Chem. Soc.*, 2015, **137**, 9417–9422.
34 Q. Wei, J.-W. Cheng, C. He and G.-Y. Yang, *Inorg. Chem.*, 2014, **53**, 11757–11763.
35 H. Zhang, M. Zhang, S. Pan, Z. Yang, Z. Wang, Q. Bian, X. Hou, H. Yu, F. Zhang, K. Wu, F. Yang, Q. Peng, Z. Xu, K. B. Chang and K. R. Poeppelmeier, *Cryst. Growth Des.*, 2015, **15**, 523–529.
36 Z. Chen, S. Pan, Z. Yang, X. Dong, X. Su and Y. Yang, *J. Mater. Sci.*, 2013, **48**, 2590–2596.
37 E. L. Belokoneva, Y. K. Kabalov, O. V. Dimitrova and S. Y. Stefanovich, *Crystallogr. Rep.*, 2003, **48**, 44–48.
38 Y. Z. Huang, L. M. Wu, X. T. Wu, L. H. Li, L. Chen and Y. F. Zhang, *J. Am. Chem. Soc.*, 2010, **132**, 12788–12789.
39 Q. Jing, X. Dong, X. Chen, Z. Yang, S. Pan and C. Lei, *Chem. Phys.*, 2015, **453–454**, 42–46.
40 J. Ferrara and E. Reinheimer, *Acta Crystallogr., Sect. A: Found. Adv.*, 2017, **73**, C1133.
41 G. Sheldrick, *Acta Crystallogr., Sect. A: Found. Adv.*, 2015, **71**, 3–8.
42 G. M. Sheldrick, *Acta Crystallogr., Sect. C: Struct. Chem.*, 2015, **71**, 3–8.
43 S. K. Kurtz and T. T. Perry, *J. Appl. Phys.*, 1968, **39**, 3798–3813.
44 S. J. Clark, M. D. Segall, C. J. Pickard, P. J. Hasnip, M. I. J. Probert, K. Refson and M. C. Payne, *Z. Kristallogr. – Cryst. Mater.*, 2005, **220**, 567–570.
45 P. Hohenberg and W. Kohn, *Phys. Rev.*, 1964, **136**, B864–B871.
46 W. Kohn and L. J. Sham, *Phys. Rev.*, 1965, **140**, A1133–A1138.
47 M. C. Payne, M. P. Teter, D. C. Allan, T. A. Arias and J. D. Joannopoulos, *Rev. Mod. Phys.*, 1992, **64**, 1045–1097.
48 J. P. Perdew, K. Burke and M. Ernzerhof, *Phys. Rev. Lett.*, 1996, **77**, 3865–3868.
49 J. S. Lin, A. Qteish, M. C. Payne and V. Heine, *Phys. Rev. B: Condens. Matter Mater. Phys.*, 1993, **47**, 4174–4180.
50 J. Yan, D. Chu, Z. Chen and J. Han, *Inorg. Chem.*, 2022, **61**, 18795–18801.
51 G. Zou, C. Lin, H. Jo, G. Nam, T.-S. You and K. M. Ok, *Angew. Chem., Int. Ed.*, 2016, **55**, 12078–12082.
52 H. Yu, N. Z. Koocher, J. M. Rondinelli and P. S. Halasyamani, *Angew. Chem., Int. Ed.*, 2018, **57**, 6100–6103.